19th Brazilian Congress of Thermal Sciences and Engineering
November 6th–10th, 2022, Bento Gonçalves - RS - Brazil

ENC-2022-0423
NUMERICAL STUDY OF A 1M DIAMETER METHANOL POOL FIRE: AN ASSESSMENT OF TURBULENCE AND EVAPORATION MODELS

William Oliveira
Raphael Machado Cezar
Universidade Federal do Rio Grande do Sul – UFRGS, Departamento de Engenharia Mecânica (DEMEC), R. Sarmento Leite, 425 - Centro Histórico, Porto Alegre - RS, 90050-170.
williamoliveira0409@gmail.com, raphael.cezar@hotmail.com
Felipe Roman Centeno
Universidade Federal do Rio Grande do Sul – UFRGS, Departamento de Engenharia Mecânica (DEMEC), R. Sarmento Leite, 425 - Centro Histórico, Porto Alegre - RS, 90050-170.
frcenteno@mecanica.ufrgs.br
Guilherme Henrique Fiorot
Universidade Federal do Rio Grande do Sul – UFRGS, Departamento de Engenharia Mecânica (DEMEC), R. Sarmento Leite, 425 - Centro Histórico, Porto Alegre - RS, 90050-170.
guilherme.fiorot@ufrgs.br

Abstract. *The numerical modeling of fire is a study of great interest to understand the characteristics of the flame and its heat released into the environment. In the present study, six numerical models of methanol combustion in a 1 m diameter pool fire are evaluated, based on experimental studies from the literature, to identify the best numerical setup for modeling the physical process employing the temperature distribution and the heat flux. The simulations differ by the turbulence model – Deardorff, Dynamic Smagorinsky, and Constant Smagorinsky – and the Heat Release Rate (HRR) of the methanol's combustion form – prescribed and modeled. The temperature and heat flux sensors have the same configuration and position as the reference experiment. The computer simulation is performed in FDS (Fire Dynamics Simulator). The results showed that depending on the measurement position analyzed and the HRR modeling, the turbulence model can either correctly predict the pool fire behavior or reproduce incongruities to the problem's physics.*

Keywords: *FDS, Heat Release Rate, methanol, pool fire, turbulence modeling.*

1. INTRODUCTION

The validation of a numerical model procedure compares experimental and numerical results. Simulations applying a set of parameters and hypotheses aiming to properly model the physical phenomena provide the results that quantify the numerical accuracy. In problems involving combustion processes, it is a common practice to publish studies with controlled fire experiments like Sahu *et al.* (2019) and Sung *et al.* (2021). These works aim to provide accurate data about the phenomenon for a subsequent proposal of a numerical model with comparable results to the experimental ones, such as the study of Ahmed and Trouvé (2021). They are relevant to understanding fire modeling and provide a benchmark for further applications of turbulence models in more specific cases. Stewart *et al.* (2021) and Diab *et al.* (2018) present examples of these applications. The latter focuses on the turbulence phenomena and diffusion of fire whirls by applying numerical and experimental analysis. Furthermore, evaluating which model to implement in computational fluid dynamics is crucial and relevant in protection engineering scenarios such as urban, industrial, or forest fires.

This work proposes an evaluation of turbulence modeling for a $1\,\mathrm{m}$ diameter pool fire of methanol. The comparable data used to validate the phenomena comes from the experimental study of Sung *et al.* (2021), which consists of temperature and heat flux measurements in a methanol pool fire with equivalent dimensions. The numerical models submitted to the simulation are Deardorff, Constant Smagorinsky, and Dynamic Smagorinsky. These models are well-known and commonly used in fire simulations. The simulation software applied in this study is the FDS (Fire Dynamic Simulator). It uses large-eddy simulation (LES) methodology, where the effect of the large scales is directly computed, and only models small subgrid scales.

Besides, to enhance the turbulence analysis, this work also focuses on the modeling of the Heat Release Rate (HRR) from the combustion process. Two HRR approaches are applied, using three turbulence models at a time. The first

approach consists in prescribing an HRR constant value: the same as the one observed by Sung *et al.* (2021). The other one considers the properties of the methanol liquid, which leads to an HRR that varies over time. To calculate the latter the evaporation process is set by the FDS to estimate the HRR generated during the simulation time.

The objective is to understand which HRR modeling and turbulence model can achieve better comparable results to the experimental ones by evaluating the energy balance, temperature, and heat flux distribution inside the domain. It is expected that a specific model among those used presents better results. Temperature and heat flux simulation sensors have the same experimental study positions. Alongside these devices, velocity and kinetic energy sensors evaluate the mesh's quality and the resolution of the turbulence scales over the pool.

2. METHODOLOGY

2.1 Experimental data from Sung *et al.* (2021)

This work is based on the study made by Sung *et al.* (2021), where a circular steel pan with an inner diameter of $1\,\mathrm{m}$, a depth of $0.15\,\mathrm{m}$, and a wall thickness of $0.0016\,\mathrm{m}$ held the methanol liquid. The burner is mounted on water-cooled cinder blocks, such that the burner rim is about $0.3\,\mathrm{m}$ above the floor. A fuel overflow basin included for safety extended $3\,\mathrm{cm}$ beyond the burner wall at its base. The fuel inlet was insulated and covered with a reflective foil to prevent preheating of the fuel. The experiment-measured properties are the starting point for the comparison and accuracy evaluation of the numerical results, such as the HRR. Table 1 presents these results.

Table 1: Experimental data from Sung *et al.* (2021).

Average flame height [m]	1.10 ± 0.22
Mass burning rate, $\dot{m}$ [g/s]	12.8 ± 0.9
Ideal Heat Release Rate, Q [kW]	254 ± 19
Heat Release Rate from calorimetry, Q_a [kW]	256 ± 45
Total Heat Release Rate radiative fraction, χ_{rad}	$0.21 \pm 16\%$

2.2 Software and hardware used in this study

The numerical simulation uses the software FDS, version 6.7.6. The FDS solves numerically the Navier–Stokes equations adapted to buoyancy-driven low Mach numbers ($Ma < 0.3$) using LES methodology. Besides, it applies a lumped species approach with a second-order scheme in time and space. The solution is obtained through the Finite Volume Method (FVM) with a gray gas model (by default) to solve the Radiative Transfer Equation (RTE) in the form of source terms. The Technical Reference Guide (McGrattan, 2013) presents more information regarding the numerical approach implemented with FDS. The hardware used in the numerical simulation of all the models is an Intel® CORE™ I7:7500U with 2,70 GHz and a RAM of 8Gb, the operating system is Windows 10 64 bits.

The post-processing of the simulation output measuring results uses Python (3.8.10) scripts. The following libraries are imported into the Python scripts: Matplotlib (Hunter, 2007) for graphical plotting, Pandas (McKinney *et al.*, 2010) for working with the output simulation file format (comma-separated values) and Numpy (Harris *et al.*, 2020) for the array operations involving multidimensional arrays, as seen in Eq. (2). The section Results presents the comparison between the turbulence and HRR models using MTR, Energy Balance, Temperature, and Heat Flux.

2.3 Parameters for assessing mesh quality

At simulations involving the study of buoyant plumes, a measure of how well the flow field is solved is given by the non-dimensional expression in $D^*/\delta x$, where δx is the nominal size of a mesh cell and D^* is a *characteristic fire diameter*, represented by Eq. (1).

$$D^* = \left(\frac{\dot{Q}}{\rho_\infty c_p T_\infty \sqrt{g}} \right)^{\frac{2}{5}} \tag{1}$$

where $\dot{Q}$ is the total HRR of the fire, ρ_∞ the fluid density, c_p the air specific heat, T_∞ the ambient surrounding temperature, and g the acceleration due to gravity forces. In this study, these variables are equal to 256 kW, 1.1839 kg/m^3,1.012 kJ/kg·K, 298 K, and 9.81 m/s^2, respectively. The recommended ratio between the characteristic fire diameter D^* and the grid size δ_x falls inside a 4-16 range (McGrattan *et al.*, 2020).

Equation (2) represents the scalar quantity referred to as the Measure of Turbulence Resolution (MTR), where the angled brackets are suitable time-averages and k_{sgs} is the subgrid kinetic energy. Pope (2004) specifies an acceptable

value of $MTR \leq 0.2$ in adaptive LES, which corresponds to the resolution of at least 80% of the kinetic energy.

$$MTR(x) = \frac{\langle k_{sgs} \rangle}{\langle TKE \rangle + \langle k_{sgs} \rangle} \tag{2}$$

The Turbulent Kinetic Energy (TKE) is computed by Eq. (3).

$$TKE = \frac{1}{2}\left((\tilde{u} - \langle \tilde{u} \rangle)^2 + (\tilde{v} - \langle \tilde{v} \rangle)^2 + (\tilde{w} - \langle \tilde{w} \rangle)^2\right) \tag{3}$$

The work from Ciani and Gai (2018) shows that it is possible to use the Pearson coefficient (r) to quantify the correlation (linear dependence) between two variables X and Y, where $\bar{X}$ and $\bar{Y}$ are the mean values of the sample, to establish the quality of the grid resolution in thermo-fluid dynamics simulations. Eq. (4).

$$r = \frac{\sum_{i=1}^{n}\left(X_i - \bar{X}\right)\left(Y_i - \bar{Y}\right)}{\sum_{i=1}^{n}\sqrt{\left(X_i - \bar{X}\right)^2}\sqrt{\left(Y_i - \bar{Y}\right)^2}} \tag{4}$$

This Pearson's Coefficient (PC) can be used to assess the X-Y correlation where X and Y are the time-averaged values of the output quantities of the same fire scenario, such as the temperature, but at different grid resolutions. This indicator gives additional information to evaluate the solution convergence, and a value of 0.75 or greater, in modulus, is recommended.

2.4 Geometry and Mesh

In this study, the domain was configured as a $5\,\mathrm{m}$ cube, and the boundary conditions were defined as open, except for the one that represents the floor which was set as an adiabatic surface. The pool's base is centralized and placed over a $0.3\,\mathrm{m}$ adiabatic obstruction with a $1\,\mathrm{m}$ length and width. The geometry was built in FDS. The software does not allow the design of circular surfaces since it is based only on cartesian geometries. As the pool in the experiment is circular with a diameter of $1\,\mathrm{m}$, a cartesian approximation was conducted based on the area of the pool fire. A circular vent configuration was also used. This procedure creates a similar geometry by adding the cells with their centroid inside the defined radius. However, it would not be possible to verify the exact surface area – created to adapt the prescribed HRR. The pool geometry and the mesh are shown in Fig. 1. The experiment pool's area, conducted by Sung *et al.* (2021), is $0.785\,\mathrm{m}^2$ and the one obtained by the cartesian approximation is $0.79\,\mathrm{m}^2$ – a difference of $0.58\,\%$.

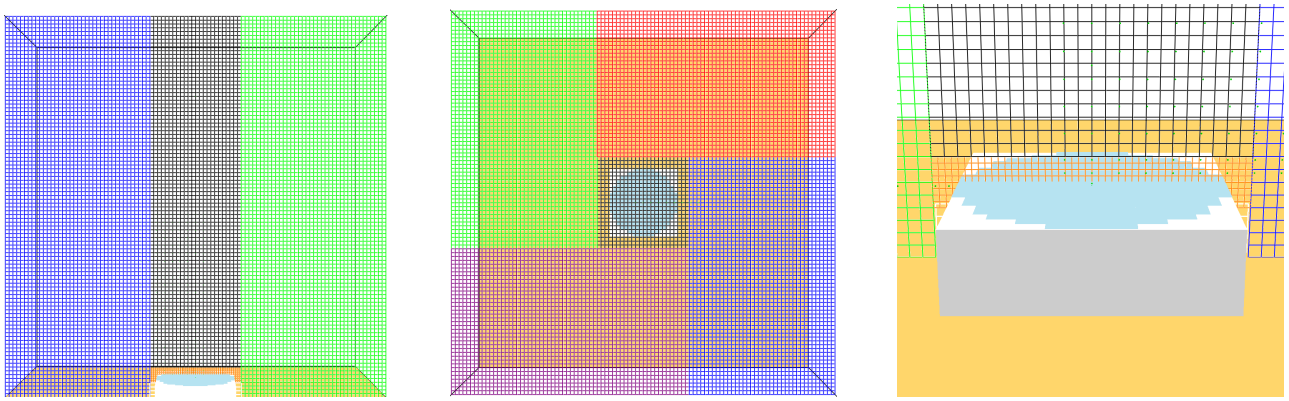

(a) (b) (c)

Figure 1: Views of the mesh applied in this work. (a) Side view on plane xz. (b) Top view on plane xy. The mesh is divided into five regions to enable the parallel simulation. (c) Detailed view of the pool's surface showing the refinement of $2.5\,\mathrm{cm}$.

The mesh pattern used in the simulations for the numerical validation divides the domain into two regions: one external to the fire with a constant $\delta x = 5\,\mathrm{cm}$ and another part that concerns the pool fire region, varying δx. This last part takes the horizontal limit of the pool fire over $0.1\,\mathrm{m}$ for each side and the vertical extension. All cells have a cubic form. Table 2 presents the nominal size, the total number of cells, and the computational cost for each mesh grid used.

Figure 2 shows the recommended values for solution convergence in the literature for Grids 1 to 3. Figure 2a brings the recommended region for a definition of the grid resolution. Both Grid 1 and Grid 2 are inside the recommended convergence region. Grid 2 presents a lower MTR than Grid 1, and its ratio value is more centered. Following these

Table 2: Simulation parameters for each mesh used.

Mesh	δ_x [cm]	Cells	Total CPU Time
Grid1	10	6,912	4 h 10 min
Grid2	5	55,296	7 h 42 min
Grid3	2.5	442,368	26 h 2 min

criteria, the second grid would be the best mesh. However, the mesh setting procedure must consider other parameters and characteristics. For example, although Grid 3 falls outside this region, it has the lowest MTR value and could be used as a final mesh since the ratio value is less significant when compared to the MTR value. Figure 2b presents the Pearson's Coefficient (PC) recommended value, represented by the gray line $r = 0.75$. All samples have a direct correlation since all of them are positives. This PC parameter brings additional information for convergence of the model by evaluating if the subsequent mesh refinements are strongly correlated. The literature recommends a minimum $\mid r \mid \geq 0.75$ for the samples to be considered similar. The variable used for the correlation analysis in Eq. (4) is the temperature. From the refinement from Grid 1 to Grid 2 (r_{12}), the first two samples along the vertical domain, the ones closer to the pool fire, have values below the line of 0.75. However, in the refinement from Grid 2 to Grid 3 (r_{23}), all samples have a high correlation factor range. It means that the numerical results between Grids 2 and 3 are statistically similar, even with a lower MTR value for Grid 3. And since Grid 2 presented a simulation time shorter than Grid 3, Grid 2 is the final mesh selected.

After this study, a more detailed and precise optimization for the final mesh configuration was adopted to guarantee a better evaporation modeling for the HRR modeled case, based on a refinement of the region more proximate to the pool surface, with a characteristic length of $\delta x = 2.5$ cm, as seen in Fig. 1c. The outer-region of the fire has cubic volumes of $\delta x = 5$ cm as selected from the mesh study. A coarser mesh region was set below the pool surface. This procedure reduces the simulation time for regions that don't have relevance in this study since the obstruction is considered adiabatic. This configuration can be observed in Fig. 1a and Fig. 1b.

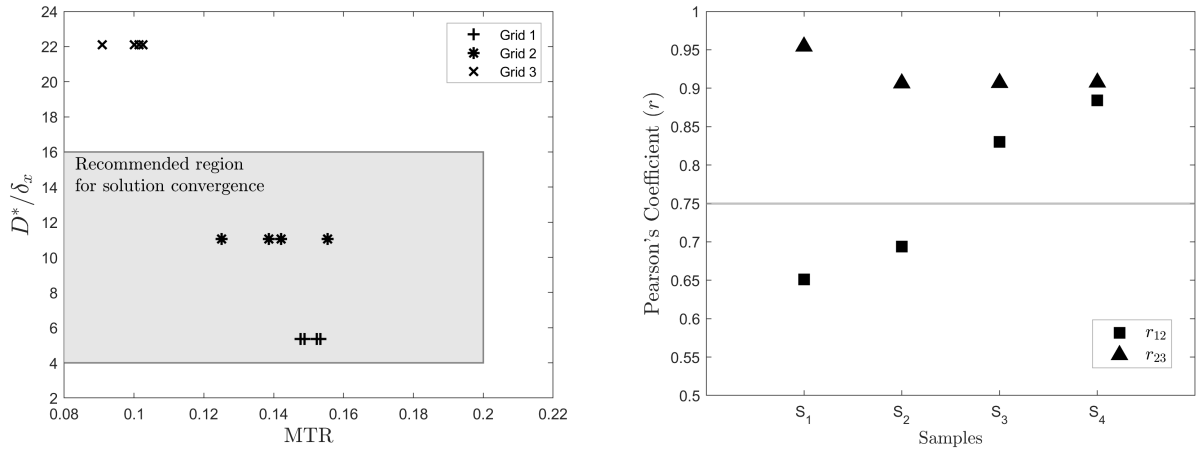

(a) (b)

Figure 2: (a) Convergence recommended region. Samples at $z = 160$ cm, $z = 200$ cm, $z = 240$ cm, and $z = 280$ cm, the points going from right to left order on the same grid. (b) Pearson's Coefficient evaluation. S_1 at $z = 40$ cm, S_2 at $z = 60$ cm, S_3 at $z = 180$ cm, and S_4 at $z = 200$ cm.

2.5 Devices

FDS allows the placement of measuring instruments. Sensors capture different simulation parameters – the temperature, the heat flux, the kinetic energy, and the velocity – at positions equivalent to the experiment; additional measure points for analysis improvement are also implemented. The thermocouples sensors measure the gas temperature and are arranged on the right side of the pool, from $0.1\,\mathrm{m}$ to $0.7\,\mathrm{m}$ in the x-direction, and $0.35\,\mathrm{m}$ to $2.40\,\mathrm{m}$ (spaced by $0.1\,\mathrm{m}$ each) in the z-direction – except for the ones at $0.35\,\mathrm{m}$ over the pool. To estimate the MTR value at each temperature sensor and to ensure the resolution of the vortexes in those regions, all points with temperature sensors have one kinetic energy sensor and three velocity sensors, one for each coordinate u, v, and w. The heat flux sensors are positioned radially and vertically (on the wall and over the pool). Their arrangement along the domain can be identified in Fig. 3.

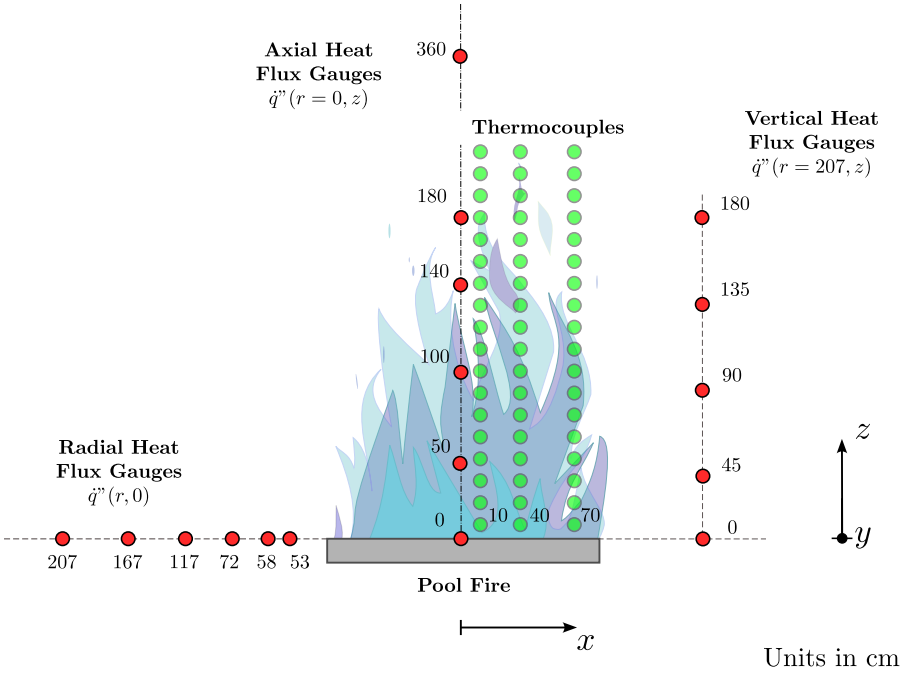

Figure 3: Pool fire schematic diagram with distribution of temperature and heat flux the sensors.

2.6 Energy balance

The energy balance of the methanol combustion process in a pool fire is presented to ensure the agreement to the first law of thermodynamics. It can be defined by the study of Chan Kim *et al.* (2019) applying Eq. (5),

$$\dot{Q}_a = \dot{Q}_r + \dot{Q}_c + \dot{Q}_s + \dot{Q}_b \tag{5}$$

where $\dot{Q}_a$ is the power emitted by the flame, $\dot{Q}_r$ is the radiation emitted to the environment, $\dot{Q}_c$ is the heat emitted by sensible convection from the flame, $\dot{Q}_s$ is the heat redirected to the pool, and $\dot{Q}_b$ is the loss from the burner.

2.7 Heat Release Rate and fire modeling

As previously mentioned, two HRR approaches in FDS are applied. Both models were simulated using three turbulence models each. The first is by modeling the HRR based on the properties of methanol liquid. The values considered in the modeling of methanol are presented in Tab. 3 based on the studies of Carlson and Westrum (1971), Goodwin (1987) and Vargaftik (1975). In this case, the evaporation phenomenon has to be taken into account and is modeled considering the radiative fraction of the heat released by the flame. The portion of the heat emitted, in the form of radiation, is $21\,\%$. Part of this heat emitted by the flame heats the pool, improving the combustion process. The other method involves a prescribed HRR of $256\,\mathrm{kW}$, obtained by the experiment, to model the burning of methanol in the pool. This type of approach is simpler since heat release is already prescribed. The simulation time was set to $60\,\mathrm{s}$ based on pool fire numerical analysis that shows a stabilization region for HRR achieved to prescribed and modeled cases when applying the Deardorff model. The solution for additional simulation time intervals was not performed due to computational limitations.

Table 3: Methanol properties for modeled HRR.

Emissivity	1
Density [kg/m^3]	796
Absorption coefficient	1500
Heat of reaction [kJ/kg]	1099
Conductivity [W/mK]	0.20
Specific heat [kJ/kgK]	2.48
Boiling Temperature [°C]	64.65

2.8 Turbulence models

This work uses three turbulence models available on the FDS software. The LES is implemented to model the subgrid-scale (SGS) turbulence and the turbulence model is applied to the closure of the SGS flux terms. In FDS, gradient diffusion is the turbulence model used to close both the SGS *momentum* and scalar flux terms. A model for the turbulent transport coefficient is then required: the turbulent (eddy) viscosity or the turbulent (eddy) diffusivity. The latter is obtained using a constant Schmidt number (for mass diffusivity) or a Prandtl number (for thermal diffusivity). The turbulent viscosity, μ_t, is the most important coefficient (McGrattan, 2013). There are five turbulence models available in the FDS software version utilized: Constant Smagorinsky, Dynamic Smagorinsky, Deardorff, Vreman, and WALE. The Vreman model is similar to the Dynamic Smagorinsky model, and the WALE model (Wall-Adapting Local Eddy-Viscosity) is applied to capture the eddy viscosity in the first off-wall grid cell – not valid for this work since near-wall effects are not related. The mathematical formulation is properly described in FDS's Technical Guide.

2.8.1 Deardorff

The Deardorff turbulence model was initially applied in works related to meteorology. For example, the numerical analysis of the mixed-layers inside Stratocumulus capped clouds (Deardorff, 1980) is one of the first applications of this model. It is based on subgrid kinetic energy, k_{sgs}. Models with a kinetic energy approach tend to perform better than models based only on resolved scale information. Equation (6) presents the eddy viscosity calculation,

$$\mu_{LES} = \rho\, C_v \Delta \sqrt{k_{sgs}} \quad , \qquad C_v = 0.1 \tag{6}$$

where Δ is the filter width, $\Delta = (\delta x \delta y \delta z)^{1/3}$, and C_v is the Deardorff constant. The subgrid kinetic energy is represented by Eq. (7),

$$k_{sgs} = \frac{1}{2}\left((\bar{u} - \hat{u})^2 + (\bar{v} - \hat{v})^2 + (\bar{w} - \hat{w})^2\right) \tag{7}$$

where $\bar{u}$ is the average value of u at the grid cell center and $\hat{u}$ is a weighted average of u over adjacent cells, as describe Equations (8a) and (8b).

$$\bar{u}_{ijk} = \frac{u_{ijk} + u_{i-1,jk}}{2} \tag{8a}$$

$$\hat{u}_{ijk} = \frac{\bar{u}_{ijk}}{2} + \frac{\bar{u}_{i-1,jk} + \bar{u}_{i+1,jk}}{4} \tag{8b}$$

The terms $\hat{v}$ and $\hat{w}$ are defined similarly.

2.8.2 Constant Smagorinsky

The Smagorinsky turbulence model was introduced by (Smagorinsky, 1963) to model geophysical flows and meteorology problems as well. The Smagorinsky model assumes a high Reynolds number to guarantee that the energy is transferred from the large to the small scales, classical to LES approaches. Considering this, small scales, defined by the filtering scale, show only dissipation of momentum. Equation (9) presents the viscosity μ_{LES} modeled as,

$$\begin{aligned} &\mu_{LES} = \rho\,(C_s\Delta)^2 \left(2S_{ij}S_{ij} - \frac{2}{3}(\nabla\cdot\mathbf{u})^2\right)^{\frac{1}{2}} \quad , \qquad C_s = 0.2 \\ &\text{with } S_{ij} \equiv \frac{1}{2}\left(\frac{\partial u_i}{\partial x_j} + \frac{\partial u_j}{\partial x_i}\right), \end{aligned} \tag{9}$$

where S_{ij} is the large-scale strain-rate tensor and C_s is the Smagorinsky constant. The value for this constant defined in Eq. (9) comes from Lilly (1967) study and assumes that the production of scales is equal to its dissipation.

2.8.3 Dynamic Smagorinsky

The Dynamic Smagorinsky model, originally developed for engineering flows, is based on an algebraic identity between the subgrid-scale stresses at two different filtered levels and the resolved turbulent stresses. For this model, the coefficient C_s in Eq. (9) is no longer taken as a constant, but rather computed on local flow conditions. The coefficient is obtained dynamically as the calculations progress. This procedure exploits the spectral information on the energy content of the smallest resolved scales provided by LES calculations to dynamically adjust the model (Germano *et al.*, 1991). This dynamic model is known to deliver better spatial convergence and resolution independence when compared to nondynamic models (Kirkpatrick *et al.*, 2006).

3. RESULTS

3.1 MTR evaluation

Figures 4a to 4f show the MTR simulation results for both prescribed and modeled approaches at three radial distances from the center of the pool fire: $x = 0.1$ m $x = 0.4$ m, and $x = 0.7$ m. Depending on the measurement position, a specific turbulence model presents better performance, that is, a desirable range of $MTR \leq 0.2$ is obtained. Except for regions very close to the pool fire surface, most of the values are below this value. Considering the prescribed HRR, the Deardorff turbulence model presented the lowest MTR values for samples at $x = 0.1$ m, and $x = 0.4$ m – Fig.4a and 4b respectively. However, for $x = 0.7$, the resolution of the turbulence scales is better captured by the Dynamic Smagorinsky turbulence model. On the other hand, now considering a modeled HRR approach, the desirable range of MTR is achieved by the Deardorff model at $x = 0.4$ m and by the Dynamic one at $x = 0.1$ m, and $x = 0.7$ m. Except for Fig. 4b and Fig. 4e, the Constant Smagorinsky presented the higher MTR values, for both prescribed and modeled cases. From these results, it is possible to infer that for the outermost x-range evaluated, the MTR is properly calculated by Deardorff and Dynamic Smagorinsky turbulence models. Seen that the Deardorff model represents good MTR values for all samples, this is the turbulence model that provides better information regarding the fire modeling.

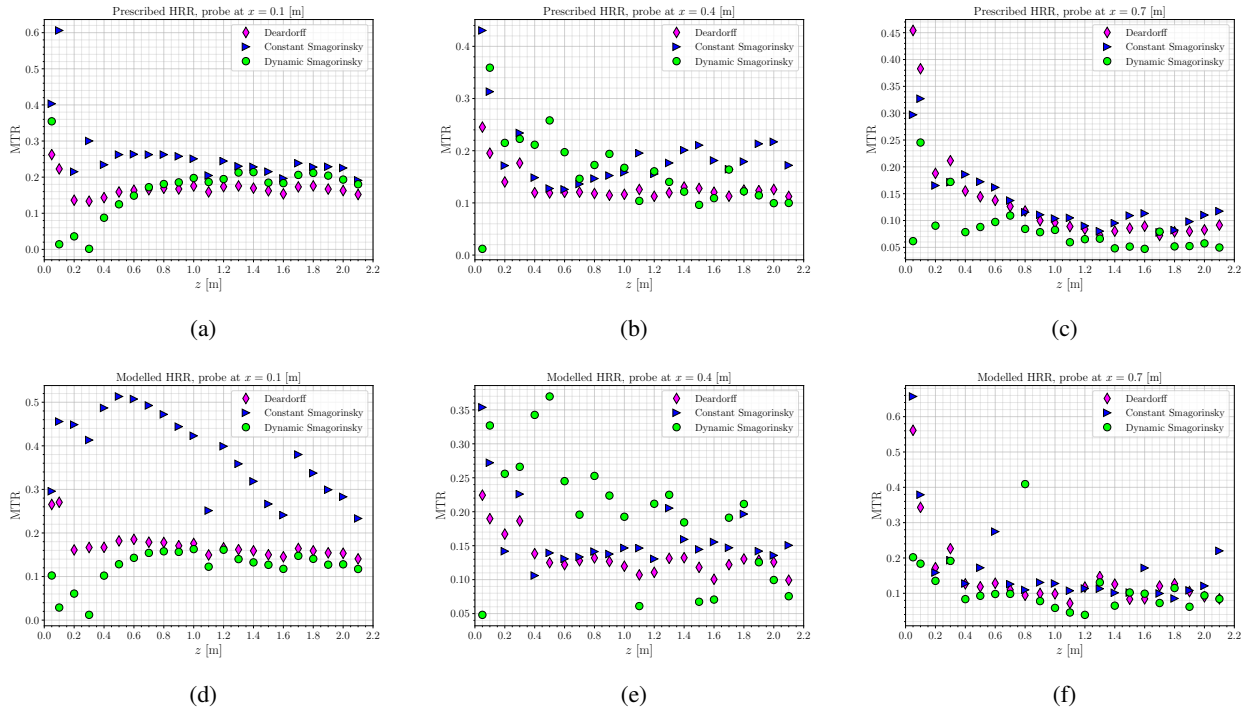

Figure 4: MTR for different radial distances from the centerline along the z-axis. (a)-(c) Prescribed HRR case. (d)-(f) Modeled HRR case.

3.2 Energy balance

Figure 5 presents the results from Eq. (5) on both HRR approaches obtained by default as FDS outputs. Figure 5a shows for the Prescribed HRR case that the energy balance is verified for all turbulence models. However, for the modeled approach the energy balance result was different from expected, Fig. 5b. The Deardorff model presents values different from zero, but the convergence is verified at 15 W. The Constant and Dynamic Smagorinsky models presented unsatisfactory results since the energy balance is not attended and it tends to grow at the time interval.

3.3 Heat release rate

The HRR is shown in Fig. 6 for both prescribed and modeled cases with the turbulence simulated models. Figure 6a shows that the HRR from all turbulence models falls in the range measured by the experiment of Sung *et al.*. Figure 6b, however, presents this condition only for the Deardorff turbulence model.

The mean value of the HRR for the prescribed case is $206.29\,\mathrm{kW}$. This value is lower when compared to the mean one obtained by Sung *et al.*. However, all HRR turbulence model results are similar. The HRR for the modeled approach

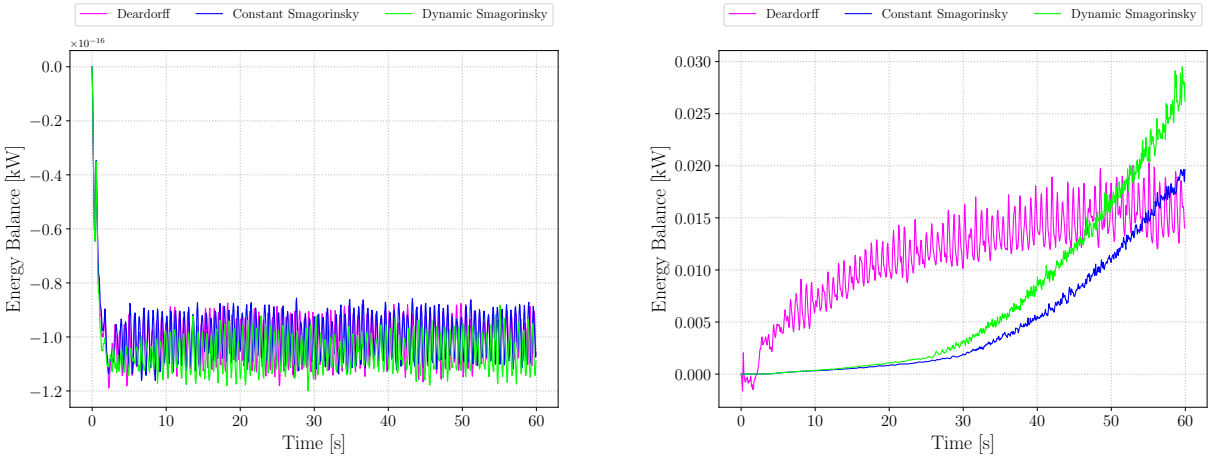

(a) (b)

Figure 5: Energy balance of the three turbulence models simulated. (a) Prescribed HRR case. (b) Modeled HRR case.

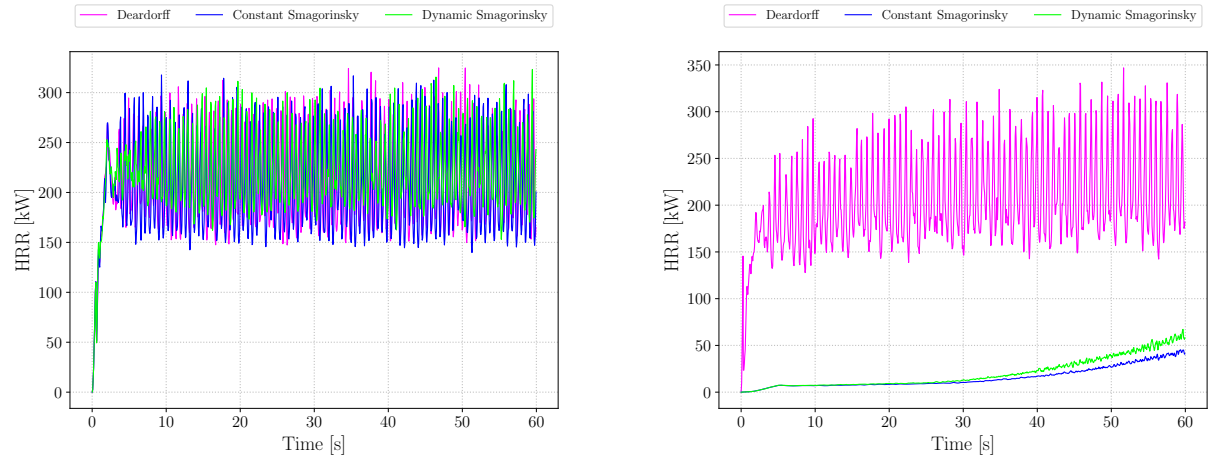

(a) (b)

Figure 6: HRR for the Deardorff, Constant and Dynamic Smagorinsky turbulence models. (a) Prescribed HRR case. (b) Modeled HRR case.

confirms what was visualized in Fig. 5b: in the simulation time interval, except for the Deardorff model which presented HRR stable after 10 s, the two other models presented lower HRR values that are still developing. Due to computational limitations, the simulation time was not increased to evaluate the stabilization region for the modeled HRR.

3.4 Gas temperature

3.4.1 Axial distribution of gas temperature

Figure 7 presents the gas temperature results for the turbulence models, based on the prescribed and modeled HRR approaches. The results are measured at the center of the flame by varying the axial distance above the pool fire surface and compared with the experimental data obtained by Sung *et al.* at the same position. For each analysis, the markers represent the time interval average temperatures and the upper and lower limits correspond to the time interval standard deviation.

Note that for the prescribed HRR approach in Fig. 7a the mean results among the turbulence models are very close, having similar standard deviations as well. The temperature profile is also similar to the experimental one, with most of the simulated results falling inside the temperature standard deviation region from experiments. For distances greater than $100\,\mathrm{cm}$, the turbulence models properly capture the gas temperature, with values proximate to the experimental ones. Inside the fire level, which corresponds to a z <1.10 m, the measured values are different – although the simulation temperature profile is as expected. This divergence can be a result of the HRR's lowest value.

In the other approach, Fig. 7b, a similar temperature distribution is observed for the Deardorff turbulence model but presents lower mean temperature values in the region close to the pool. However, it converges with the experimental

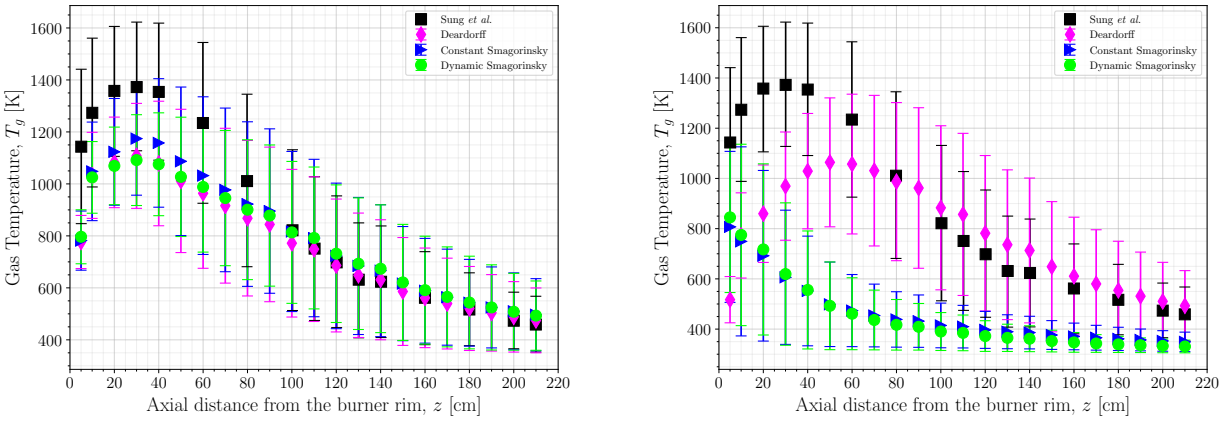

(a) (b)

Figure 7: Gas temperature over the burner rim. (a) Prescribed HRR case. (b) Modeled HRR case.

one starting at 80 cm over the pool. The Constant and Dynamic Smagorinsky models are similar to each other but show temperatures far below the experimental. A possible explanation for this behavior near the surface of the pool is the evaporation effect taken into account for the modeled HRR approach. A part of the flame heat is redirected back to the pool, and not to the environment.

3.4.2 Gas temperature through time

Figures 8a and 8b present the gas temperature variation between the 40-42 s time interval for prescribed and modeled approaches – the same time interval presented in the work of Sung *et al.*. The experiment results were organized by mean and standard deviation values, corresponding to the figure's gray region which is limited by both upper and lower standard deviations. This procedure can facilitate the evaluation of how well the temperature results by each model are proximate to the experimental results.

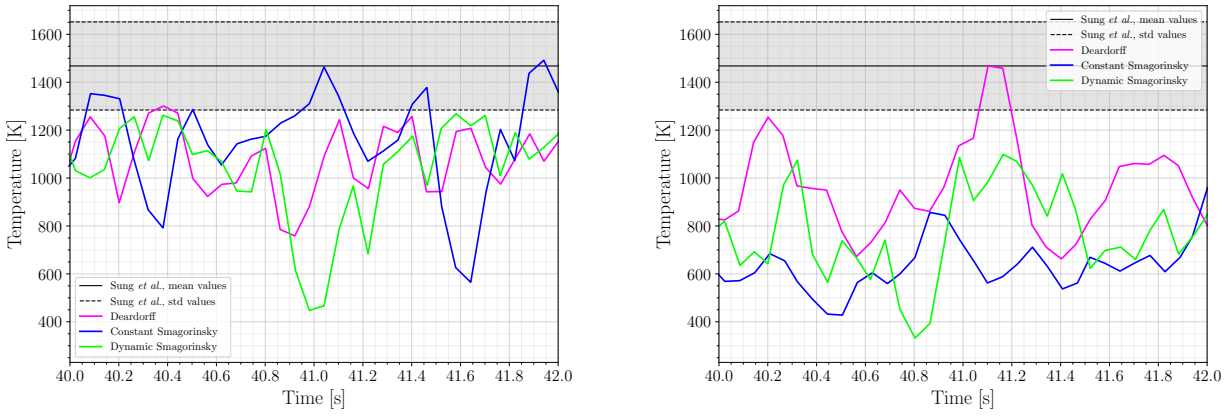

(a) (b)

Figure 8: Gas temperature from 40 s to 42 s, at $r = 0$ and $z = 30$ cm. (a) Prescribed HRR case. (b) Modeled HRR case.

Note that in both cases, the results obtained for all turbulence models are mostly lower than the experimental ones. In the case of the modeled HRR, the average temperatures are the lowest. For the presented time interval of 2 s, it can be seen that only the Constant Smagorinsky model in the prescribed case and the Deardorff model in the modeled one reach the mean value of the experiment.

3.5 Heat flux

3.5.1 Radial distribution of heat flux

Figure 9 presents the heat flux results at the sensors located at the same height as the pool surface and distributed along the x-axis. Each turbulence model is compared with the experimental results of Sung *et al.* (2021) and Klassen and Gore (1994). Klassen and Gore results are used in Sung *et al.* as a reference comparison. They reported on the flame height and the heat flux distribution near 1.0 m diameter pool fires burning several fuels, including methanol. The former used the same burner as the latter, but with a $5\,\mathrm{mm}$ (rather than $10\,\mathrm{mm}$) lip height.

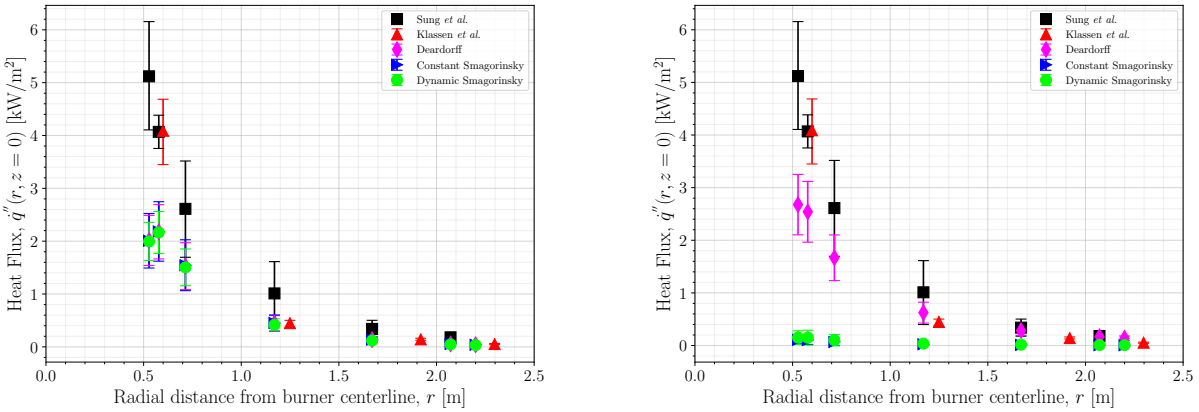

(a) (b)

Figure 9: Radial heat flux from burner centerline. (a) Prescribed HRR case. (b) Modeled HRR case.

Figure 9a shows the results for the prescribed HRR case. The three numerical model values are similar in both mean and standard deviation. However, these values are smaller than the experimental ones in the region near the flame. The modeling shows convergence with the experimental data at only $0.7\,\mathrm{m}$ from the pool. For the modeled HRR case in Fig. 9b, the Deardorff is the only model able to describe the heat flux distribution, showing values similar to that resulting from the experimental data. Suitable modeling can be guaranteed over $0.7\,\mathrm{m}$ from the surface. The heat flux obtained by the Constant and Dynamic Smagorinsky models is practically invariant to the presence of the flame, returning values close to zero.

3.5.2 Axial distribution of Heat Flux

Figures 10a and 10b show the behavior of the heat flux along the z-axis at $r = 207$ cm for both prescribed and modeled cases, respectively. The heat flux sensors are oriented in the direction of the pool. In both approaches, all the

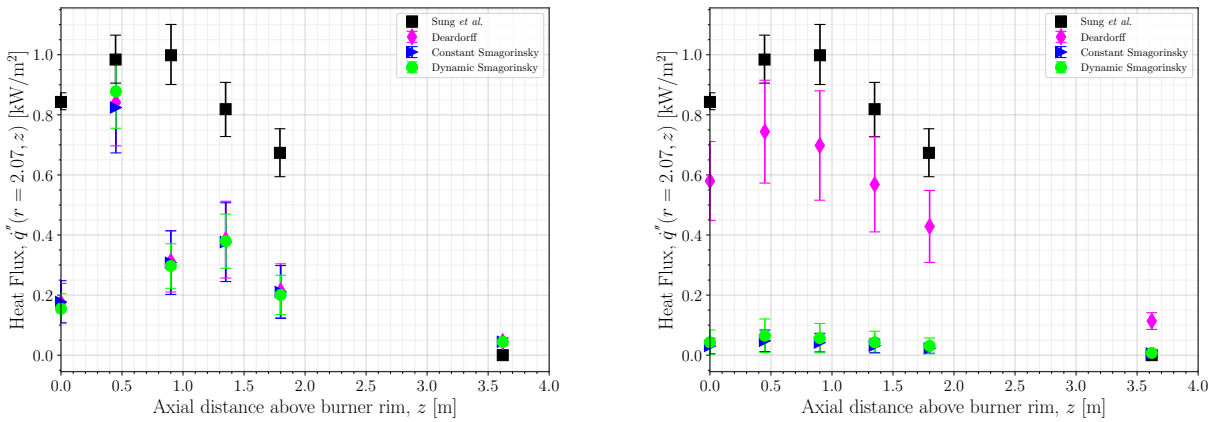

(a) (b)

Figure 10: Axial heat flux from burner centerline. (a) Prescribed HRR case. (b) Modeled HRR case.

values obtained were lower than the Sung *et al.* ones. In the prescribed case all turbulence models had similar behavior with minor deviation from each other but converged in only two points with the experimental one. For the modeled HRR case, it is possible the observation of suitable modeling by Deardorff, even with a high standard deviation. The Constant and Dynamic Smagorinsky models did not show relevant variations with the flame presence. The same behavior was observed for the radial case in Fig. 9b but for different turbulence models.

4. CONCLUSION

The numerical simulation implemented in this work tried to reproduce a case from the literature in which temperature, burning rate, and heat release rate measurements characterize a 1 m diameter methanol pool fire. The simulation applies three different turbulence models along with two HRR modeling approaches. The correct prediction of pool fire physics depends on the measurement position analyzed and the value of HRR.

The prescribed HRR approach leads to better results. For all turbulence models, achieving the energy balance. The mean HRR is equivalent to the experimental, and the gas temperature curves converge with the experiment. Depending on the evaluation, the Constant – gas temperature near the pool – and Dynamic Smagorinsky – MTR values – present slightly better results than the Deardorff ones. The modeled HRR approach leads to some uncertainties when applying the Constant and Dynamic Smagorinsky models. The axial gas temperature and the radial heat flux measurements of the Deardorff turbulence model are similar to the experiments. This model is also the only turbulence model that stabilizes the HRR in the time interval of the simulation.

Some evaluations can be made for future work. As seen, depending on the measurement position inside the domain, alongside the model's configuration, the software source code should be well-arranged for this problem specifically: for a given combination of HRR and turbulence modeling, the domain should be divided into regions that are properly captured by this optimum combination.

5. ACKNOWLEDGMENTS

This research was financially supported by the Brazilian CAPES, CNPq, and FAPERGS institutions.

6. REFERENCES

Ahmed, M.M. and Trouvé, A., 2021. "Large eddy simulation of the unstable flame structure and gas-to-liquid thermal feedback in a medium-scale methanol pool fire". *Combustion and Flame*, Vol. 225, pp. 237–254. ISSN 0010-2180. doi:/10.1016/j.combustflame.2020.10.055.

Carlson, H.G. and Westrum, E.F., 1971. "Methanol: Heat capacity, enthalpies of transition and melting, and thermodynamic properties from 5–300°k". *The Journal of Chemical Physics*, Vol. 54, No. 4, pp. 1464–1471. doi:10.1063/1.1675039.

Chan Kim, S., Lee, K.Y. and Hamins, A., 2019. "Energy balance in medium-scale methanol, ethanol, and acetone pool fires". *Fire Safety Journal*, Vol. 107, pp. 44–53. ISSN 0379-7112. doi:/10.1016/j.firesaf.2019.01.004.

Ciani, F.S. and Gai, G., 2018. "Indicators for the Quality Assessment of the Grid Resolution". *Journal of Physics: Conference Series*, Vol. 1107, No. 4. ISSN 17426596. doi:10.1088/1742-6596/1107/4/042025.

Deardorff, J.W., 1980. "Stratocumulus-capped mixed layers derived from a three-dimensional model". *Boundary-Layer Meteorology*, Vol. 18, pp. 495–527. doi:/10.1007/BF00119502.

Diab, M., Yip, A., Hadavand, M., Haelssig, J. and Pegg, M., 2018. "Experimental and numerical comparison of small-scale gaseous fire whirls". *Journal of Physics: Conference Series*, Vol. 1107, p. 042032. doi:10.1088/1742-6596/1107/4/042032.

Germano, M., Piomelli, U., Moin, P. and Cabot, W.H., 1991. "A dynamic subgrid-scale eddy viscosity model". *Physics of Fluids A*, Vol. 3, No. 7, pp. 1760–1765. ISSN 08998213. doi:10.1063/1.857955.

Goodwin, R.D., 1987. "Methanol thermodynamic properties from 176 to 673 k at pressures to 700 bar". *Journal of Physical and Chemical Reference Data*, Vol. 16, No. 4, pp. 799–892. doi:10.1063/1.555786.

Harris, C.R., Millman, K.J., van der Walt, S.J., Gommers, R., Virtanen, P., Cournapeau, D., Wieser, E., Taylor, J., Berg, S., Smith, N.J., Kern, R., Picus, M., Hoyer, S., van Kerkwijk, M.H., Brett, M., Haldane, A., del Río, J.F., Wiebe, M., Peterson, P., Gérard-Marchant, P., Sheppard, K., Reddy, T., Weckesser, W., Abbasi, H., Gohlke, C. and Oliphant, T.E., 2020. "Array programming with NumPy". *Nature*, Vol. 585, No. 7825, pp. 357–362. doi:10.1038/s41586-020-2649-2. URL `https://doi.org/10.1038/s41586-020-2649-2`.

Hunter, J.D., 2007. "Matplotlib: A 2d graphics environment". *Computing in Science & Engineering*, Vol. 9, No. 3, pp. 90–95. doi:10.1109/MCSE.2007.55.

Kirkpatrick, M.P., Ackerman, A.S., Stevens, D.E. and Mansour, N.N., 2006. "On the application of the dynamic smagorinsky model to large-eddy simulations of the cloud-topped atmospheric boundary layer". *Journal of the Atmospheric Sciences*, Vol. 63, No. 2, pp. 526–546. doi:10.1175/JAS3651.1.

Klassen, M. and Gore, J., 1994. *Structure and radiation properties of pool fires*. NIST.

Lilly, D.K., 1967. "The representation of small-scale turbulence in numerical simulation experiments". *IBM Form*, pp. 195–210. doi:/10.5065/D62R3PMM.

McGrattan, K., 2013. "Fire Dynamics Simulator (version 6) Technical Reference Guide, NISTSP1018". *Nist Special Publication*, Vol. 1.

McGrattan, K., Hostikka, S., McDermott, R., Floyd, J., Weinschenk, C. and Overhold, K., 2020. "Sixth Edition Fire Dynamics Simulator User's Guide (FDS)". *NIST Special Publication 1019*, Vol. Sixth Edit.

McKinney, W. *et al.*, 2010. "Data structures for statistical computing in python". In *Proceedings of the 9th Python in Science Conference*. Austin, TX, Vol. 445, pp. 51–56.

Pope, S.B., 2004. "Ten questions concerning the large-eddy simulation of turbulent flows". *New Journal of Physics*, Vol. 6. ISSN 13672630. doi:10.1088/1367-2630/6/1/035.

Sahu, D., Jain, S., Gupta, A. and Kumar, S., 2019. "Experimental studies on different liquid pool fires inside the compartment". *Fire Safety Journal*, Vol. 109, p. 102858. ISSN 0379-7112. doi:10.1016/j.firesaf.2019.102858.

Smagorinsky, J., 1963. "General circulation experiments with the primitive equations". *Monthly Weather Review*, Vol. 91, No. 3, p. 99. doi:10.1175/1520-0493(1963)091<0099:GCEWTP>2.3.CO;2.

Stewart, J.R., Phylaktou, H.N., Andrews, G.E. and Burns, A.D., 2021. "Evaluation of cfd simulations of transient pool fire burning rates". *Journal of Loss Prevention in the Process Industries*, Vol. 71, p. 104495. ISSN 0950-4230. doi:/10.1016/j.jlp.2021.104495.

Sung, K., Chen, J., Bundy, M. and Hamins, A., 2021. "The characteristics of a 1m methanol pool fire". *Fire Safety Journal*, Vol. 120. ISSN 03797112. doi:10.1016/j.firesaf.2020.103121.

Vargaftik, N., 1975. *Handbook of Physical Properties of Liquids and Gases. Pure Substances and Mixtures*. Hemisphere, Washington, 2nd edition.

7. RESPONSIBILITY NOTICE

The authors are solely responsible for the printed material included in this paper.